JOURNAL OF SPACECRAFT AND ROCKETS
Vol. 44, No. 1, January–February 2007

Coast-Arc Orbit Stability During Spiral-Down Trajectories About Irregularly Shaped Bodies

Matthew A. Wissler,* David B. Spencer,† and Robert G. Melton‡
Pennsylvania State University, University Park, Pennsylvania 16802

DOI: 10.2514/1.24995

The orbit stability for a spacecraft while in a minimum propellant, optimal low-thrust transfer from a high-altitude orbit to low-altitude orbit around an irregularly shaped body is addressed. To ensure the spacecraft's safety, it is necessary to know that if the spacecraft's main engines safe during the period of orbit transfer, then the resulting coast orbit is stable or unstable with low-probability of the spacecraft colliding with the body or escaping from orbit. To answer this question, a Monte Carlo simulation, developed in FORTRAN 90, was developed to analyze a sufficiently large set of coast orbits under the influence of a high-fidelity gravitational model. The perturbations arising from the nonspherical harmonics were derived using Hotine's partially nonsingular geopotential formulation. This method was chosen because of the higher efficiency of Hotine's method when compared with using a spherical harmonic analysis. The simulation examines the orbital radius to determine the danger of spacecraft crash or escape.

Nomenclature

a	=	semimajor axis, km
$\boldsymbol{a}$	=	gravitational acceleration vector, km/s^2
a_α	=	gravitational acceleration component, where α is x, y, or z, km/s^2
C^α_{nm}, S^α_{nm}	=	Hotine directional gravitational coefficients
C_{nm}, S_{nm}	=	normalized gravitational coefficients
e	=	eccentricity
e max	=	maximum eccentricity before orbit becomes unstable
$f^{1,2,3}_{nm}$	=	Hotine scaling factors
G	=	universal gravitational constant, km^3/kg $\cdot$ s^2
i	=	inclination, deg
J_2	=	$-C_{20}$, second zonal coefficient
J_3	=	$-C_{30}$, third zonal coefficient
J_4	=	$-C_{40}$, fourth zonal coefficient
M	=	mass of body, kg
$N_{\max}$	=	maximum order of the harmonic expansion of the gravitational potential
P_{nm}	=	associated Legendre function
$\bar{P}_{nm}$	=	normalized associated Legendre function
$\boldsymbol{r}$	=	position vector in inertial space, km
r_0	=	initial radius, km
R_{body}	=	largest principal axis of the body, km
U	=	gravitational potential, km^2/s^2
U_α	=	directional derivative of U, where α is x, y, or z, km^2/s^2
U_{body}	=	U of body, km^2/s^2
x, y, z	=	position components in inertial frame, km
λ	=	latitude, rad
μ_{body}	=	gravitational parameter of the body, km^3/s^2
ϕ	=	longitude, rad
!!	=	factorial of odd integers

Received 8 May 2006; revision received 13 September 2006; accepted for publication 25 September 2006.

*Graduate Research Assistant, Department of Aerospace Engineering, 229 Hammond Building. Student Member AIAA.

†Associate Professor, Department of Aerospace Engineering, 229 Hammond Building. Associate Fellow AIAA.

‡Professor, Department of Aerospace Engineering, 229 Hammond Building. Associate Fellow AIAA.

I. Introduction

THE orbit stability of a spacecraft performing a low-thrust, minimum-propellant, optimal spiral-down orbit around a rotating, irregularly shaped body is addressed. From a safety standpoint, should the spacecraft's low-thrust propulsion system fail during this transfer, the question of whether the spacecraft may ultimately crash into the body or escape from orbit around the body is addressed in this paper. An example transfer for the Dawn spacecraft's spiral trajectory around the asteroid Vesta is shown. A capability to model the spacecraft's orbit during a loss of spacecraft thrust, for various orbit state vector initial conditions during the orbit transfer, is desired to determine the effects of the body's gravity field that includes the gravitational perturbations. These perturbations can have a significant impact on the geometry and safety of the spacecraft's orbit over time. Even if control is not lost, the gravitational perturbations will affect the orbital behavior. These perturbations will cause changes in the osculating orbital elements over time, and uncontrolled changes in semimajor axis and eccentricity may produce the undesirable effect of causing the spacecraft to either collide with the body or escape from orbit around the body.

An optimized low-thrust orbit transfer is given as a basis for the coast orbit initial conditions. As a linear stability analysis based upon the eigenvalues of the state transition matrix quickly became ill-conditioned due to the presence of fast variables of integration, a more direct numerical method was necessary to determine the stability of the space between the higher and lower orbits [1]. To effectively explore the space, a sufficient number of the states along this transfer were used as independent initial conditions for coast orbits that would result from loss of spacecraft thrusting at that point in the orbit transfer. These initial conditions are used with a fourth-order Runge–Kutta orbit propagator with a fifth-order adaptive stepsize control that propagates each specific coast orbit into the future (thirty days into the future was used in the Dawn example). A time history of the orbital elements is recorded and the values of minimum radius are found. The minimum radius that the spacecraft obtains during the 30 days of coasting is compared with the maximum radius of body that acts as an exclusion zone. If the minimum orbital radius penetrates into the exclusion zone then collision with the body is possible. If the maximum radius is larger than the value for the sphere of influence, then escape is assumed. Obviously, either case would precipitate a possible change in the designed transfer trajectory to eliminate the chance of these situations occurring. The goal of this thorough search of the space around the low-thrust transfer trajectory is to map a safe area for the spacecraft in case of malfunction. This sample was investigated for

various degree and order gravity field models to assess the added value of increased fidelity.

The analysis tool implements the gravitational potential and corresponding perturbing accelerations from a nonspherical body's gravity field using Hotine's recursion method [2], and uses an orbit propagation algorithm that will provide a time history of the spacecraft's osculating elements. Whereas this tool is applicable to the gravity field of any body, an example optimal spiral-down trajectory using Vesta's gravity field is studied.

II. Dynamical Equations of Motion

The dynamical equations of motion for the three-dimensional two-body problem with perturbing accelerations are

$$\ddot{\boldsymbol{r}} = -\frac{GM_{\text{body}}\boldsymbol{r}}{r^3} + \boldsymbol{a} \tag{1}$$

where

$$\boldsymbol{r} = x\hat{\boldsymbol{i}} + y\hat{\boldsymbol{j}} + z\hat{\boldsymbol{k}} \tag{2}$$

$$\boldsymbol{a} = \nabla U_{\text{body}} \tag{3}$$

$$U_{\text{body}} = \frac{\mu_{\text{body}}}{r}\sum_{n=0}^{\infty}\left(\frac{R_{\text{body}}}{r}\right)^n \sum_{m=0}^{n} \bar{P}_{nm}(\sin\phi)(\bar{C}_{nm}\cos m\lambda + \bar{S}_{nm}\sin m\lambda) \tag{4}$$

and

$$r = \sqrt{x^2 + y^2 + z^2} \tag{5}$$

By reduction of order, we express these as a system of six first-order ordinary differential equations.

III. Review of Literature

The problem of orbit stability is not a new one, however, the special case of a spacecraft orbiting close to a highly nonspherical body like an asteroid complicates matters. The highly nonspherical body will have a gravity field with more pronounced perturbation effects from the higher order perturbations than that of a nearly spherical body like the Earth. These perturbations have the ability to cause secular change in the osculating orbital elements like eccentricity and semimajor axis of an orbiting spacecraft.

The families of orbits considered in this paper are nearly polar and are relatively close to Vesta. A study of orbit stability research in the past for low-altitude polar orbits around asteroids by Scheeres et al. [3] notes that the perturbations due to the gravity field and the rotation of the body differ significantly from Keplerian orbits in the two-body problem. This causes large energy and angular momentum changes in very short periods of time. Hu and Sheeres [4] also define orbit stability as the situation where the orbit's size and shape are generally constant, although the orientation of the orbit around the body can change. However, they note that orbits around the orbit resonance location can change their size, shape, and orientation in a relatively short period of time [5]. Resonance is defined as an integer ratio of the period of the orbit to the rotation rate of the body. For example, a 3:4 resonance means that the body rotates 3 rotations for 4 orbits of the spacecraft. Hu and Scheeres define an instability characteristic denoted "size-shape unstable" [5]. Here, the orbit's semimajor axis and eccentricity are not constant on average and can lead to impact or escape.

Scheeres et al. [6] also define a variable called e max, which is an analytic prediction of what the maximum eccentricity (reached after one circulation period of the periapsis) for an initially near-circular, polar orbit. Here, they used e max along with changes in semimajor axis and angular momentum to characterize unstable motion. They define e max as

$$e\max \approx \frac{10}{3}\frac{r_0^2|C_{20}|}{a^2} + \frac{r_0^3|C_{30}|}{ar_0^2|C_{20}|} \tag{6}$$

The type of numerical stability analysis used by Scheeres et al. is expanded in this paper. Higher order gravity fields of irregularly shaped bodies have been studied [6–8]. However, numerical computation grows dramatically with larger gravity field sizes and is more difficult to model. This paper, too, explores gravity field models far beyond simple 2×2 models. The unique application of the Hotine method provides quick and repeatable analysis methods for arbitrary sized gravity field models. Although this method is still computationally complex, run times vs traditional methods of calculating gravitational perturbation accelerations are reduced substantially. This allows the nontrivial higher order terms beyond 2×2 to be taken into account for these nonspherical bodies. This is an important distinction, because unlike Earth, where terms greater than second order have values that are several orders of magnitude less than J_2, irregularly shaped bodies such as Vesta have higher order terms that are only one order of magnitude less than J_2. These terms are significant and are included in this stability analysis providing a more accurate model of stability for orbits around nonspherical bodies.

IV. Hotine's Method and Geopotential Accelerations

Hotine's partially nonsingular geopotential formulation [2] is used to calculate the geopotential accelerations from the nonspherical nature of the body's geometry. This formulation is quite different from the direct analytic derivative approach for calculating geopotential accelerations. The analytic method, where the gradient of each term in the spherical harmonic expansion is calculated directly, becomes quite cumbersome for large degree and order gravity fields. In this case, it adds to the computational cost of propagation because the derivatives of the potential are roughly three times as long as the potential itself (due to the need to evaluate three components of the gradient). Hotine's method allows for the expression of the Cartesian derivatives as just another spherical harmonic expansion. This makes the evaluation of the derivatives roughly the same order as for the potential itself. Bettadpur [9] showed that an algorithm based on Hotine's method outperforms three other standard spherical harmonic derivative computation algorithms, and used it for computation of the geopotential accelerations, yielding significant savings in computation time.

Bettadpur provides a good overview of Hotine's method for calculating geopotential accelerations, which will now be summarized [9]. The associated Legendre functions can be calculated recursively: a straightforward explanation of this procedure and a numerical algorithm to perform it can be found in [10]. Using the factorial of odd integers, the recursion relationship is made up of three equations. Starting values are provided by

$$P_m^m(x) = (-1)^m(2m-1)!!(1-x^2)^{m/2} \tag{7}$$

$$P_{m+1}^m(x) = x(2m+1)P_m^m \tag{8}$$

for the general recursive relationship

$$P_n^m(x) = \frac{x(2n-1)P_{n-1}^m}{(n-m)} - \frac{(l+m-1)P_{n-2}^m}{(n-m)} \tag{9}$$

It should also be noted that this recursion relationship is for non-normalized associated Legendre functions, so any numerical results derived from them would have to be normalized for use in the spherical harmonic potential or spherical harmonic acceleration expressions. Bettadpur [9] collects the terms in the expansion by the degree and order of the solid harmonics themselves, and the expression for the spherical harmonic expansion of the derivative of the potential is shown in Eq. (10) (here, α denotes the Cartesian direction of the derivative x, y, or z):

$$U_\alpha = \frac{\mu_{\text{body}}}{R_{\text{body}}^2} \sum_{n=0}^{N_{\max}+1} \left(\frac{R_{\text{body}}}{r}\right)^{n+1} \sum_{m=0}^{n} \bar{P}_{nm}(\sin\phi) \times (\bar{C}_\alpha \cos m\lambda + \bar{S}_\alpha \sin m\lambda) \tag{10}$$

The latitude and longitude can be expressed in Cartesian coordinates as

$$\phi = \cos^{-1}\sqrt{\frac{x^2+y^2}{x^2+y^2+z^2}} \qquad \begin{matrix} 0 \le \phi \le \frac{\pi}{2} & \text{if } z \ge 0 \\ -\frac{\pi}{2} \le \phi \le 0 & \text{if } z < 0 \end{matrix} \tag{11}$$

$$\lambda = \cos^{-1}\sqrt{\frac{x^2}{x^2+y^2}} \qquad \begin{matrix} 0 < \lambda \le \pi & \text{if } y \ge 0 \\ \pi < \lambda \le 2\pi & \text{if } y < 0 \end{matrix} \tag{12}$$

The most critical step of Hotine's method is to transform the spherical harmonic coefficients into three independent sets of acceleration harmonic coefficients, one set per acceleration direction. The values for the harmonic geopotential coefficients are usually stored in the form of a lower triangular matrix of order and degree n, and the acceleration coefficients are also represented as a lower triangular matrix of order and degree $n+1$. This implies that the degree and order of the expansion grows with each successive derivative. The resulting recursive transformations are

$$\bar{C}^{\,x}_{nm} = -f^1_{nm}\bar{C}_{n-1,m-1} + f^2_{nm}\bar{C}_{n-1,m+1} \tag{13}$$

$$\bar{S}^{\,x}_{nm} = -f^1_{nm}\bar{S}_{n-1,m-1} + f^2_{nm}\bar{S}_{n-1,m+1} \tag{14}$$

$$\bar{C}^{\,y}_{nm} = f^1_{nm}\bar{S}_{n-1,m-1} + f^2_{nm}\bar{S}_{n-1,m+1} \tag{15}$$

$$\bar{S}^{\,y}_{nm} = -f^1_{nm}\bar{C}_{n-1,m-1} - f^2_{nm}\bar{C}_{n-1,m+1} \tag{16}$$

$$\bar{C}^{\,Z}_{nm} = f^3_{nm}\bar{C}_{n-1,m} \tag{17}$$

$$\bar{S}^{\,Z}_{nm} = f^3_{nm}\bar{S}_{n-1,m} \tag{18}$$

Some important exceptions occur for $m=0$ and $m=1$. For $m=0$, the $m-1$ index will create a situation where the formula attempts to reference a value outside the matrix of spherical potential values. In this case and any other cases where nonexistent values are referenced, a value of zero should be used, with two exceptions. The exception for the $m=0$ case is

$$\bar{C}^{\,x}_{n0} = f^2_{n0}\bar{C}_{n-1,1} \tag{19}$$

$$\bar{S}^{\,x}_{n0} = f^2_{n0}\bar{S}_{n-1,1} \tag{20}$$

$$\bar{C}^{\,y}_{n0} = f^2_{n0}\bar{S}_{n-1,1} \tag{21}$$

$$\bar{S}^{\,y}_{n0} = -f^2_{n0}\bar{C}_{n-1,1} \tag{22}$$

The second exception for the $m=1$ case is

$$\bar{C}^{\,x}_{n1} = -2f^1_{n1}\bar{C}_{n-1,0} + f^2_{n1}\bar{C}_{n-1,2} \tag{23}$$

$$\bar{S}^{\,x}_{n1} = -f^1_{n1}\bar{S}_{n-1,01} + f^2_{n1}\bar{S}_{n-1,2} \tag{24}$$

$$\bar{C}^{\,y}_{n1} = f^1_{n1}\bar{S}_{n-1,0} + f^2_{n1}\bar{S}_{n-1,2} \tag{25}$$

$$\bar{S}^{\,y}_{n1} = -f^1_{n1}\bar{C}_{n-1,0} - f^2_{n1}\bar{C}_{n-1,2} \tag{26}$$

The scaling factors are given by

$$f^1_{nm} = \frac{1}{2}\left(\frac{2n-1}{2n+1}(n+m)(n+m-1)\frac{1+\delta_{m0}}{1+\delta_{(1-m)0}}\right)^{\frac{1}{2}} \tag{27}$$

$$f^2_{nm} = \frac{1}{2}\left(\frac{2n-1}{2n+1}(n-m)(n-m-1)(1+\delta_{m0})\right)^{\frac{1}{2}} \tag{28}$$

$$f^3_{nm} = -\left(\frac{2n-1}{2n+1}(n+m)(n-m)\right)^{\frac{1}{2}} \tag{29}$$

It can easily be seen that by inserting the corresponding values of the spherical geopotential coefficients into the right-hand side of the recursive acceleration coefficient functions, new spherical harmonic coefficient values are formed corresponding to the particular acceleration direction. This derivation forms the basis for the Hotine method of geopotential accelerations. All of the tools are now in place to create a numerical propagation routine that will be able to generate a time history for each possible coast orbit.

V. Problem of Minimum Radius

One possible outcome produced by loss of thrust from the spacecraft's main engine is that there could be a change in eccentricity that would reduce the value of minimum orbital radius to a subsurface value. Another possible outcome would be a change in eccentricity that increases the radius over time. This effect increases as the spacecraft's orbit approaches the surface of the body. The resonance locations enhance the perturbation effects and can lead to an escape from a captured orbit, or impact.

Discrete points along the transfer trajectory from a high-altitude orbit to a low-altitude orbit are used as initial conditions for a numerical orbit propagation simulation. In this case, the resulting 30 day Cartesian state time history can be used directly to compute the magnitude of the radius. Over the 30 day coast propagation, the minimum and maximum radius values are determined. This process is repeated for a sample of the separate initial conditions in the trajectory file, and when compiled, will give a detailed view of the achieved minimum and maximum orbital radius for all possible initial conditions. The regions where there are close approaches or orbits that go below the surface of the body can be investigated in more detail by increasing the fidelity of the data over a smaller time frame centered on the area of interest. Likewise, initial conditions where escape occurs can also be studied in more depth. By using this targeted approach, it is not necessary to explore the safe areas in excruciating detail, only these areas of interest. This will ultimately save computation time.

VI. Radius Determination via Monte Carlo Simulation Structure

An example state vector file for a low-thrust transfer from the high-altitude mission orbit (HAMO) to the low-altitude mission orbit (LAMO) for the Dawn spacecraft around Vesta was obtained from Jet Propulsion Laboratory (JPL) to use as a test case. Any of these states can be used as an initial condition for a coast orbit in the simulation. Setting up the simulation in this manner allows for a large

degree of flexibility in analyzing the safety of the space surrounding the body, thereby giving the user control over the resolution of the simulation. For example, if a quick overview of the safety of the space is desired, it might only be necessary to use initial conditions every hour, but for a high-fidelity picture of periodic resonance regions, it would be helpful to have a higher resolution. It could easily be applied as a general tool to any mission where there are a known gravitational model and sample trajectory, and would be a valuable tool for general mission design.

The simulation software is written in FORTRAN 90 with a modified double precision numerical integration routine based on the Runge–Kutta 4/5 code in [10]. Because of inaccuracies in the estimated gravitational coefficients, it was felt that the Runge–Kutta 4/5 integrator was of sufficient accuracy. Thus, all simulations were done using this integrator. In an operational mission where the gravitational coeffocients were better known, a higher fidelity integrator (such as a Runge–Kutta 7/8) could be used. It uses as inputs an initial condition file containing the state vector history, in body centered inertial coordinates, and two files containing the normalized gravitational coefficients. The code numerically integrates the two-body dynamical equations of motion with perturbing accelerations derived using the Hotine method outlined previously, over a time span of 30 days. The calculated outputs are the six Cartesian states, which are then converted into osculating orbital elements and the calculated values of minimum and maximum radii for each initial condition. The values for the osculating orbital radius at all reported times are then sorted by a shell sorting algorithm. The minimum and maximum radius values for each initial condition are saved and written to a file. As the program processes the entire set of initial conditions, the results needed to generate a stability map of osculating minimum and maximum radius are generated and plotted to allow the user to see if there is any risk of crash or escape. Should these risks arise, the corresponding sets of initial conditions are recorded and a more detailed analysis can be performed.

VII. Results of Simulation

The analysis of radius, with an emphasis on the achieved maximum and minimum radius values, for a nominal mission profile of the Dawn spacecraft around the asteroid Vesta is now presented. Radius time histories are presented, as well as simulation runtime and gravity field fidelity. This is necessary because the simulation results, chosen initial condition samples, and other inputs depend upon the necessary gravity field fidelity. Sample results for both a 6×6 and a 10×10 gravity field are presented and discussed, and orbit stability is assessed. For an operational mission, such as Dawn, additional layers of the Monte Carlo simulation can be undertaken to account for other uncertainties, such as navigation errors.

The example trajectory starts as a circular orbit with an inclination of 90 deg and a radius of 950 km. The spacecraft then performs a 28 day spiral-down low-thrust trajectory to a final orbit with an inclination of 90 deg and a radius of 450 km. As the orbit design of the mission is subject to change, this is representative of the type of transfer a spacecraft can fly. In the example presented in this paper, Vesta's gravity field has been modeled with spherical harmonics up to degree and order 20. The body mass of Vesta is equal to 17.8 km^3/s^2 and the characteristic radius of Vesta is equal to 258 km. The normalized zonal coefficients ranged in order of magnitude from 10^{-1} to 10^{-5}, with $\bar{J}_2$ being the largest of the terms. The normalized sectorial terms ranged from 10^{-2} to 10^{-5}, whereas the normalized tesseral terms ranged from 10^{-2} to 10^{-7}. These coefficients were provided by NASA/JPL (data provided by Alexander Konopliv, based on data provided in [11]).

Figure 1 is a plot of inclination and orbital period vs time for the example orbit. This plot shows how the Dawn spacecraft uses the 1:1 resonance location to obtain a change in inclination without thrusting. Achieving free plane change without expending fuel is generally considered to be very desirable, as it lowers mission costs. However, there is also the inherent risk of not being able to restart the spacecraft's engines and suffering prolonged resonance effects.

A. Effects of Vesta's Gravitational Field Fidelity on Results

Before addressing the results of the stability analysis, it is necessary to analyze the order of the gravity model on the results. As the effects of the perturbations decrease with increasing order it will be beneficial to know if there is a sufficient size to closely model the perturbation effects of Vesta's shape. An important consideration when performing the osculating radius analysis was the required computation time. The example trajectory file had over 20,300 separate state vectors comprising a 28 day HAMO to LAMO transfer. This gives an average value of 120 s between each state vector. The time to analyze the coast orbits that come from propagating each of these state vectors forward in time would be prohibitive for all but the lowest fidelity gravity fields. To reduce the number of initial conditions being considered, the state vector is sampled once for every seven states along the orbit. This corresponds roughly to 10% of a LAMO orbital period, and gives a statistical sample of the data that will still provide a sufficient understanding of the space of initial conditions as a whole. This reduces the number of initial conditions to 2902. Table 1 shows normalized run time values for one initial condition case. From Table 1, the run time increases roughly exponentially as the gravity field size increases.

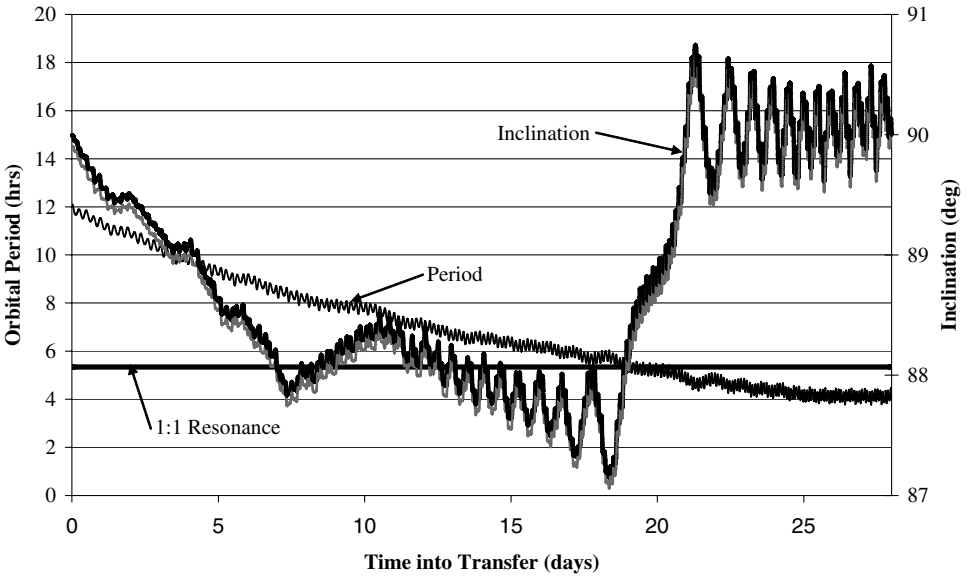

Fig. 1 Inclination vs time for example transfer orbit.

Table 1 Normalized run times for one initial condition (normalized to the 0 × 0 gravity field)

Gravity field size, n × m	Normalized run time
2 × 2	12
4 × 4	26
6 × 6	47
8 × 8	86
10 × 10	116
12 × 12	179
14 × 14	251
16 × 16	324
18 × 18	428
20 × 20	549

Table 2 Average difference of the *x* state variable between consecutively increasing gravity models

Gravity field size	Average difference, km
0 × 0	NA
2 × 2	NA
4 × 4	NA
6 × 6	126.4
8 × 8	104.7
10 × 10	118.5
12 × 12	110.4
14 × 14	94.9
16 × 16	43.8
18 × 18	12.4
20 × 20	17

It is important to understand how increasing the fidelity of the gravity field model will impact the accuracy of results. There are several approaches that can be taken to this problem. If it is necessary to know the exact location of the spacecraft 30 days into the future to assess orbit stability, then it would be necessary to use the highest fidelity gravity field model available to perform the analysis. This is not necessarily the case. As higher order terms are added into the model there will be perturbation effects acting on the spacecraft's trajectory that are not present in a lower fidelity model. If two trajectories are compared, one with a 10 × 10 gravity field model and one with a 12 × 12 gravity field model, there would be a significant deviation in the Cartesian states of each trajectory after 30 days. This would affect the quality of the knowledge of the spacecraft's location within its orbit. An analysis has been performed to show the effects of increasing the gravity field fidelity for the Dawn spacecraft around Vesta. The analysis consists of propagating a single initial condition forward in time 30 days for a variety of gravity field sizes (4 × 4, 6 × 6, 8 × 8, 10 × 10, 12 × 12, 14 × 14, 16 × 16, 18 × 18, and 20 × 20) and then comparing the corresponding history of the x position variable. Table 2 shows the actual values of the average absolute difference in the x position between consecutive gravity field sizes after 30 days of integration. This was done to show incremental changes to increasing the size of the gravity field.

The results for the next highest order gravity field are subtracted from the lower order field values, and then plotted vs time. The state history of the 30 day propagation is reported once every hour. As the fidelity of the gravity field is increased, the effect of the extra perturbations is reduced. This is mainly due to the fact that the difference between higher order gravity field coefficients is much less than that of the C_{20} and C_{30} terms. The higher order terms are often of the same magnitude, unlike the lower order terms. The best gravity field size to model in this case would be 18 × 18 as it has the lowest average difference value. It is interesting to see the nonabsolute value differences between various gravity fields. Figure 2 shows the difference between a 4 × 4 and a 6 × 6 field. It is interesting to note how quickly the two sets of results deviate from one another.

After roughly 40 h there is a large difference in the value of the x variable, and demonstrates that the higher order terms are very significant for nonspherical bodies and should not be ignored when determining stability. Figure 3 is the difference between two higher order gravity fields, 12 × 12 and 14 × 14. The difference in this plot is much lower than in Fig. 2 and there is significant divergence in the solutions after roughly 9 days. There is also no noticeable trend in the differences between 12 × 12 and 14 × 14, where the values are oscillating around a zero mean difference, and there is also less overall difference between these higher order gravity fields. Figure 4 shows the differences between two of the highest order gravity field models available for Vesta, 18 × 18 and 20 × 20. In this case, there is a dramatic increase in the time until the two models diverge, around 26 days. This supports the hypothesis that the differences between very high order gravity fields are insignificant. The lack of a difference between higher order terms implies that there is no need to use the higher order gravity fields to analyze the stability of coast orbits around Vesta.

B. Assessment of *e* max for Dawn and Vesta

One of the most critical components of orbital stability around nonspherical bodies like Vesta is the eccentricity of the orbit itself.

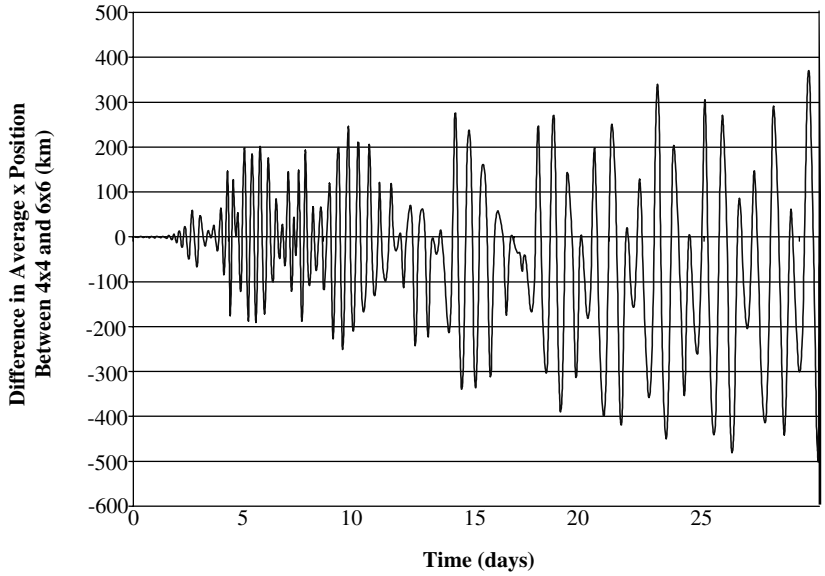

Fig. 2 Results comparison for 6 × 6 and 4 × 4 gravity models.

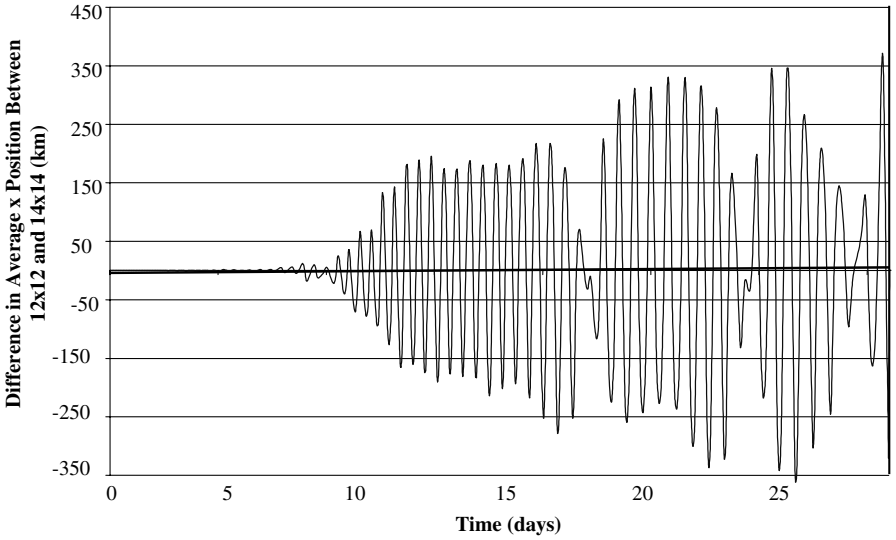

Fig. 3 Results comparison for 12 × 12 and 14 × 14 gravity models.

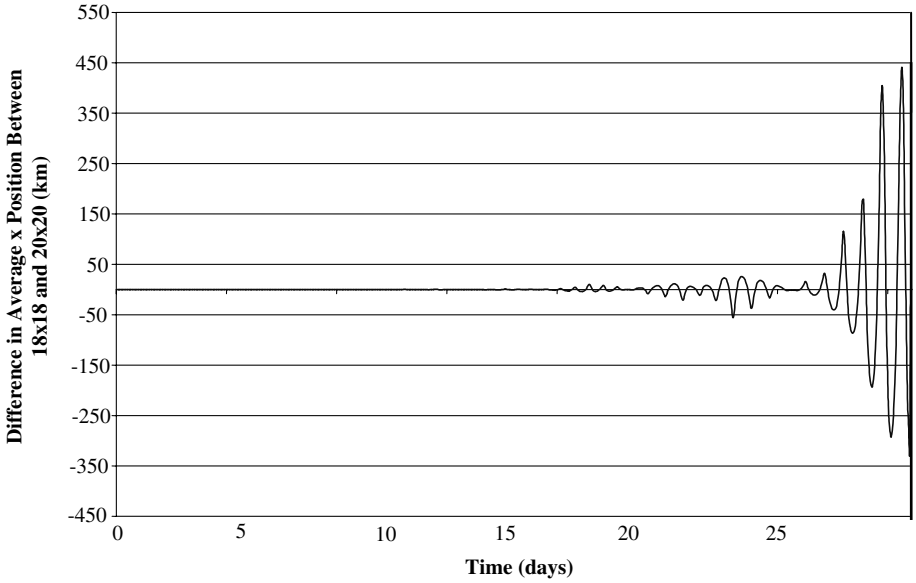

Fig. 4 Results comparison for 18 × 18 and 20 × 20 gravity models.

The eccentricity of the orbit directly affects the coupling between the gravitational perturbations and the geometry of the orbit. The term *e* max, as described earlier, is used as a measure of the maximum change in eccentricity after one circulation period of the periapsis, although exceeding this value does not necessarily imply orbit instability. To assess the stability, the periapse altitude must be assessed to indicate where the motion becomes unstable. When the value of eccentricity for any orbit around Vesta increases beyond the *e* max value, the eccentricity and the semimajor axis will begin to increase rapidly in magnitude. This behavior often leads to escape from the sphere of influence. Unfortunately, the initial conditions frequently start the coast orbits in an unfavorable environment because the initial values of *e* max are often less than the eccentricity of the orbit at the initial condition. This phenomenon for the set of initial state vectors provided in the JPL sample trajectory is shown in Fig. 5. When the individual values of initial eccentricity are subtracted from their corresponding *e* max values for all the initial conditions, it was found that 59.38% of the initial conditions are exceeding *e* max. This result points to the fact that there is going to be a similarly large number of coast trajectories escaping the sphere of influence of Vesta, and shows a possible weakness in the optimized trajectory design. Figure 6 is a similar plot to Fig. 5 except now eccentricity and *e* max are plotted vs the initial semimajor axis.

C. Minimum and Maximum Radius Results: 6 × 6 Gravity Field Case

The analysis of a sample of initial conditions for the example trajectory is now presented. The degree and order of the gravity field model was set to six and the reporting period to 1 h. The Monte Carlo analysis was run for all initial conditions, and the maximum and minimum radius were calculated for each one. These values were compiled and shown in Figs. 7 and 8. Figure 7 shows the behavior of the minimum osculating radius for all initial conditions.

Note that for this set of example data, the value of the minimum radius never goes below the characteristic radius of Vesta, indicating that there is no danger of crashing if Dawn loses thrust control at any point during the HAMO to LAMO transfer.

Figure 8 shows the maximum values of the osculating radius that were achieved for each of the initial conditions used in the simulation. These results indicate that there is a strong likelihood that the Dawn spacecraft could escape from a captured orbit around Vesta. There is a strong correlation between the altitude of the orbit and the perturbing effects of the asteroid's gravitational field. The orbit remains stable while in the higher altitude orbits but becomes unstable at the lower orbits. There are also significant effects caused by resonance locations. It can be seen from Fig. 8 that when the orbit

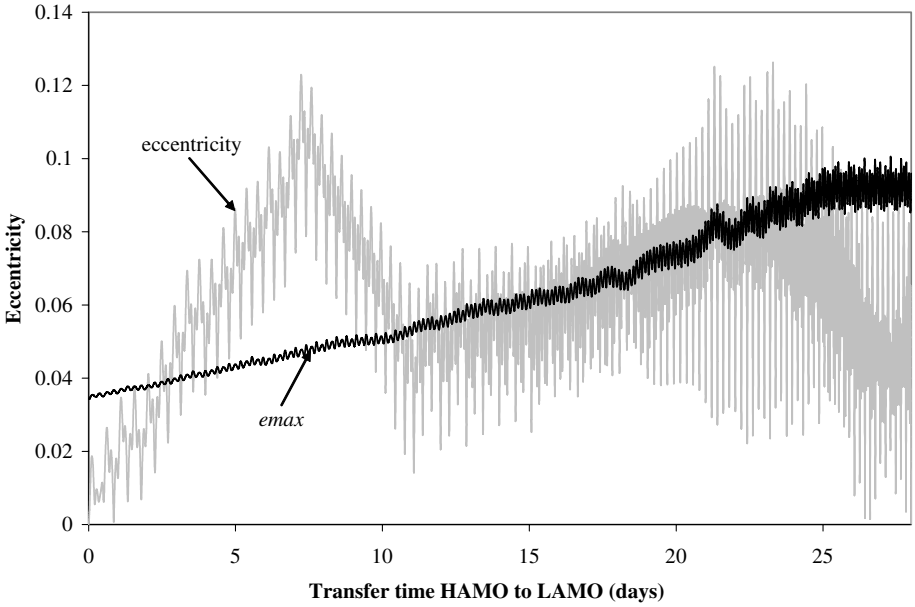

Fig. 5 Eccentricity and *e* max in the example HAMO to LAMO transfer.

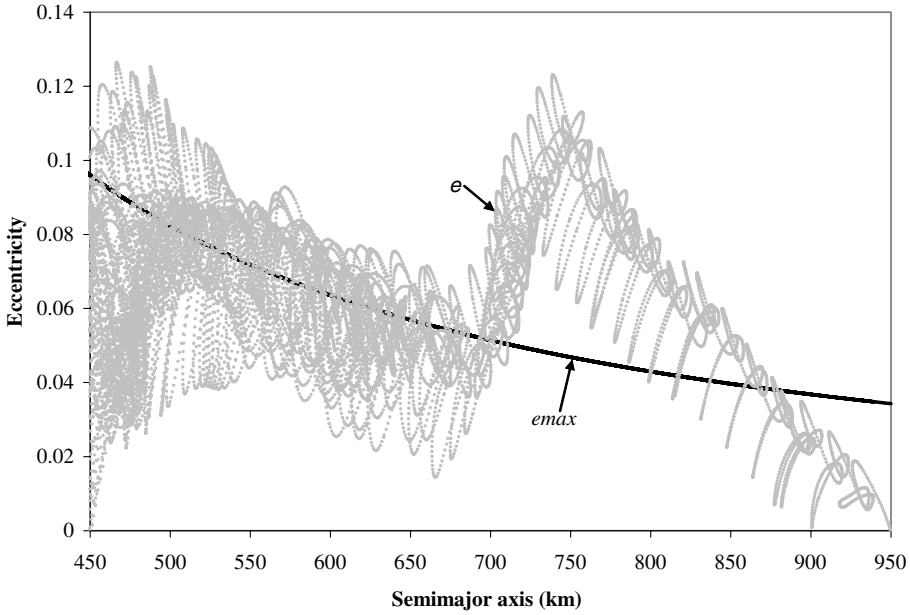

Fig. 6 Eccentricity and *e* max vs initial semimajor axis.

period coincides with regions of periodic resonance, there is an increased number of escaping trajectories. It is also very important to note the effects of the maximum eccentricity values. If Figs. 5 and 8 are compared, it can be seen that there is a direct correlation between e and e max and maximum osculating radius when $e < e$ max. When this is the case, the number of escaping trajectories falls sharply, indicating a larger number of stable orbits. These plots are very useful to determine which initial conditions merit more study and which ones are benign.

D. Periodic Resonance Effects on Orbit Stability

The effects of periodic resonance between the spacecraft orbit and the rotation rate of Vesta have a pronounced impact on the stability of the orbit. Figure 9 shows the locations of several resonance points; they are the intersection of the period line which represents the orbital period of the spacecraft's initial orbit and the resonance lines. The values of maximum orbital radius that coincide with these resonance locations are much higher than initial conditions around them. These spikes in maximum radius are caused by the enhancing effect of being located in a region of exact resonance.

The magnitude of these spikes is also increasing as the orbits get progressively closer to the surface of the asteroid. This makes sense as not only do the enhanced perturbing effects of the resonance impact the maximum radius results, but when combined with low-altitude orbits make the trajectories highly unstable. These orbit types usually lead to rapid increase in orbit eccentricity and semimajor axis and eventually escape.

E. Detailed Analysis of a Coast Orbit, $r_0 = 550$ km Example

To get better insight into how a particular coast orbit that results from a specific initial condition is behaving, it may be necessary to run a simulation that provides more detail. An abbreviated version of the main Vesta orbit stability simulation allows the user to produce results for a specific initial condition of interest, for example, a resonance location. The results shown in Fig. 10 are for an initial condition with a corresponding initial radius of 550 km. The purpose

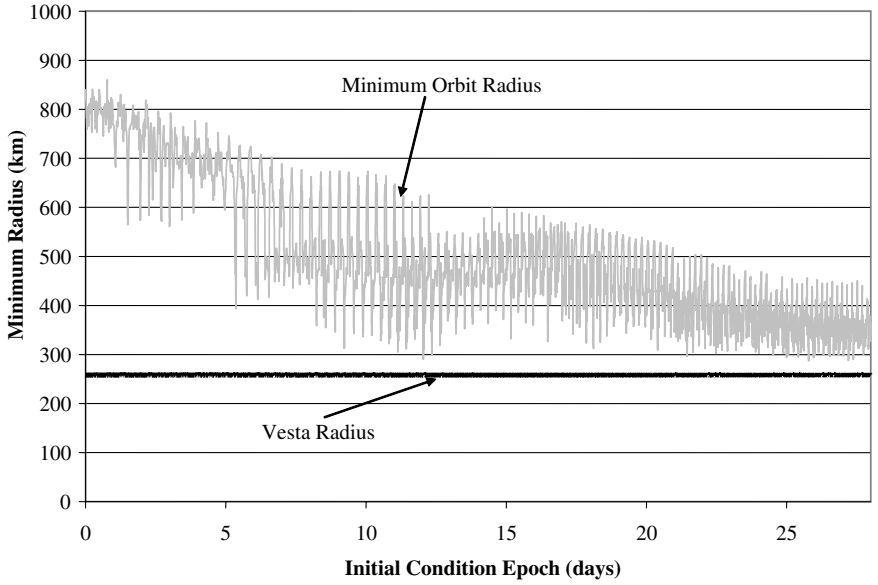

Fig. 7 Minimum radius after 30 days for 6 × 6 gravity field.

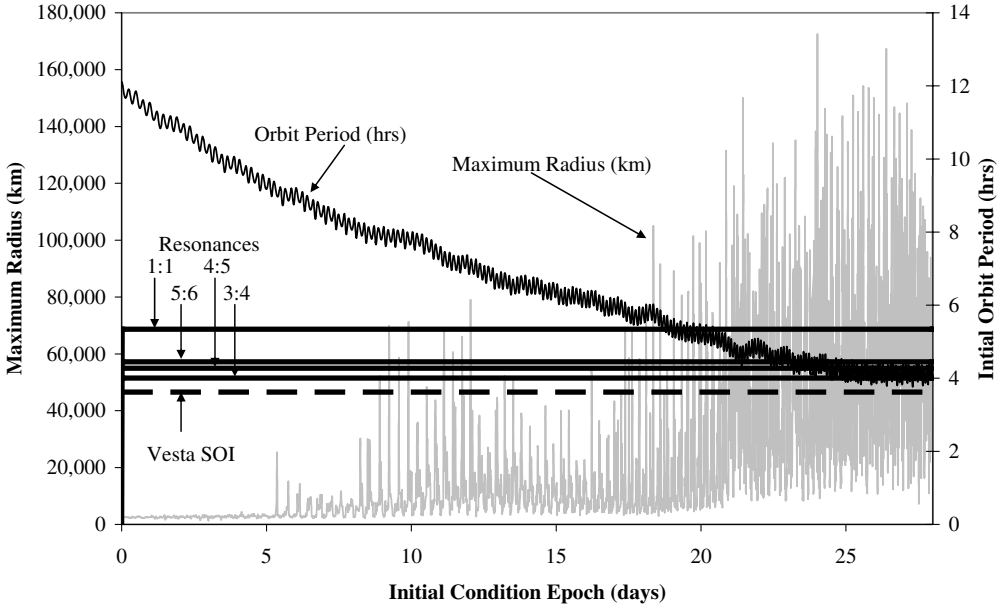

Fig. 8 Maximum radius after 30 days for 6 × 6 gravity field.

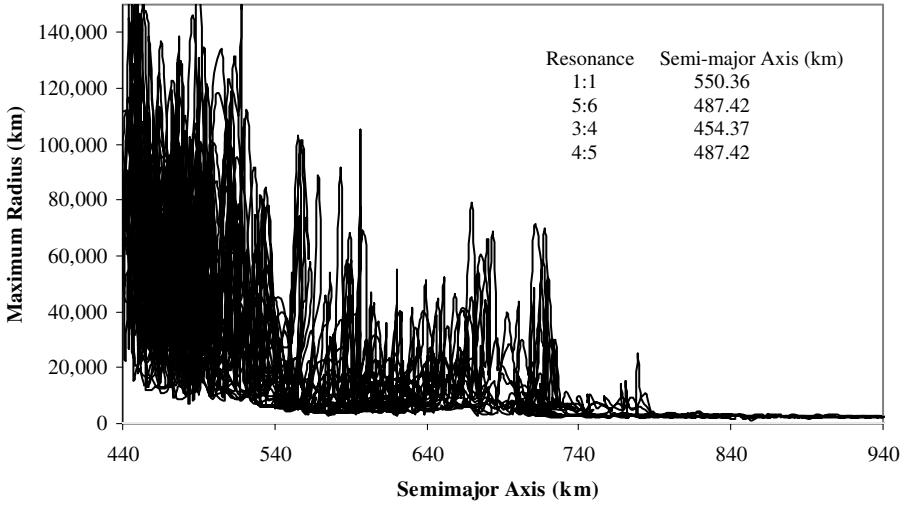

Fig. 9 Effect of orbits in periodic resonance on maximum radius.

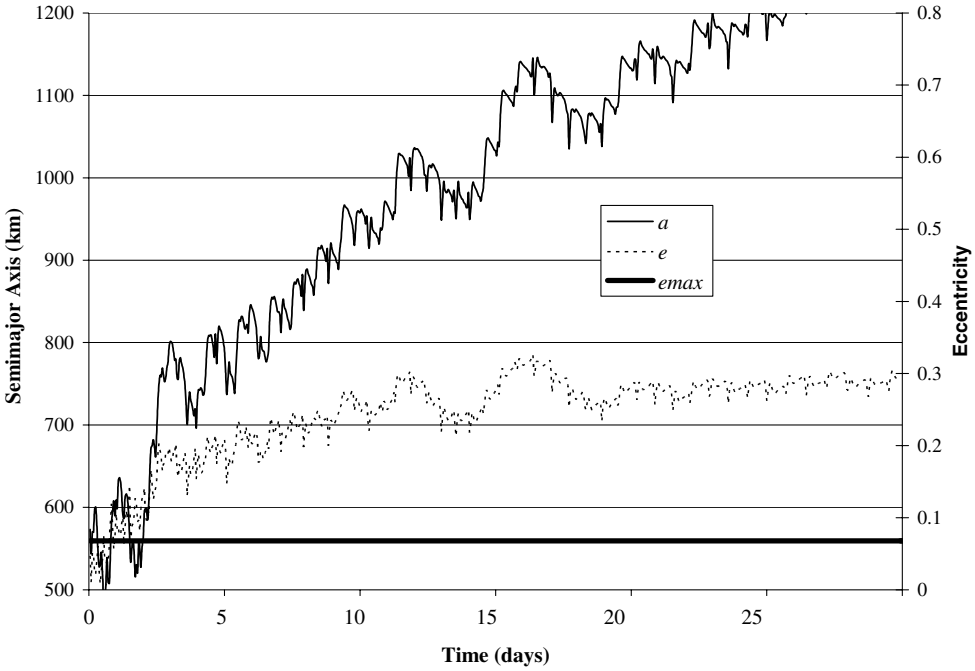

Fig. 10 Semimajor axis and eccentricity vs time.

of this plot is to show the type of results that a user can obtain for a specific initial condition. The figure shows the complete time history for all 30 days of propagation of the orbit's semimajor axis and eccentricity. The *e* max value for the initial condition was also plotted to show the change in eccentricity and semimajor axis once this threshold is crossed. It is clearly seen that there is an immediate large increase in the values of both eccentricity and semimajor axis indicating the change from a stable to unstable orbit.

VIII. Conclusions

The main value of this research is the development of a repeatable process to quickly analyze a reference trajectory near an irregularly shaped body like Vesta. Not only can the simulation provide an understanding of the stability space around the asteroid, but it can help mission designers discover potentially hazardous regions to be avoided during the actual mission. A complete mapping of minimum radius values for all of the initial conditions available has been performed for a 6×6 gravity field. It has also been shown that this field size provides sufficient fidelity to picture the stability space around the asteroid, and that Hotine's partially nonsingular geopotential formulation outperforms traditional methods of calculating gravitational accelerations due to the spherical harmonics of oblate bodies.

The overall stability and safety of the reference trajectory provided by JPL for this study has been shown to have many areas of interest. The fact that the spacecraft is located in a near polar orbit at a relatively low-altitude makes it vulnerable to the perturbing effects of Vesta's gravity field. If thruster control is lost for any reason and the spacecraft is left under only the effects of the gravitational perturbations, escape is likely for many initial conditions within the prescribed 30 day time limit. However, for this example trajectory design, there proved to be no danger of the spacecraft crashing into the surface of the asteroid.

Several conclusions can be drawn from the results of this study. First, spending the least amount of time as possible in areas of resonance during the transfer is recommended, as those regions have the most detrimental effect on orbit stability. The use of the 1:1 resonance point to acquire "free" inclination change during the orbit transfer may put the spacecraft at risk, should it be coasting during this time. Second, inducing a constraint on the orbit optimization simulation to keep the transfer orbit as close to circular as possible should be implemented. This constraint will reduce the initial eccentricity present after thrust control is lost. Having the lowest possible eccentricity will help delay the transition from a size and shape stable to an unstable orbit, thereby increasing the time until the orbit eccentricity exceeds *e* max. The eccentricity constraint provides the maximum amount of time for spacecraft controllers to regain thrust control before the spacecraft escapes from the body's sphere of influence, resulting in mission failure.

Acknowledgments

This work was supported by NASA's Jet Propulsion Laboratory under contract number 1248334. The authors would like to thank the Dawn team at Jet Propulsion Laboratory for all of their guidance throughout this entire process. We would especially like to thank Robert Werner, Joseph (Ed) Riedel, Gregory Whiffen, and Alexander Konopliv for all of their help, and for the trajectory and gravitational coefficient input files.

References

[1] Wissler, M. A., *Orbit Stability Analysis Method Applied to Trajectories for the Dawn Spacecraft Near Vesta*, Dept. of Aerospace Engineering, Pennsylvania State Univ., University Park, PA, May 2005.

[2] Hotine, M., *Mathematical Geodesy*, ESA Monograph 2, U.S. Dept. of Commerce, Washington, DC, 1969.

[3] Scheeres, D. J., Guman, M. D., and Villac, B. F., "Stability Analysis of Planetary Satellite Orbiters: Application to the Europa Orbiter," *Journal of Guidance, Control, and Dynamics*, Vol. 24, No. 4, 2001, pp. 778–787.

[4] Hu, W., and Scheeres, D. J., "Spacecraft Motion About Slowly Rotating Asteroids," *Journal of Guidance, Control, and Dynamics*, Vol. 25, No. 4, 2002, pp. 452–456.

[5] Hu, W., and Scheeres, D. J., "Numerical Determination of Stability Regions for Orbital Motion in Uniformly Rotating Second Degree and Order Gravity Fields," *Planetary and Space Science*, Vol. 52, 2004, pp. 685–692.

[6] Scheeres, D. J., Miller, J. K., and Yeomans, D. K., "Orbital Dynamics Environment of 433 Eros: A Case Study for Future Asteroid Missions," Interplanetary Network Progress Rept. 42-152, 2003.

[7] Scheeres, D. J., Ostro, S. J., Hudson, R. S., DeJong, E. M., and Suzuki, S., "Dynamics of Orbits Close to Asteroid 4179 Toutatis," *Icarus*, Vol. 132, No. 1, March 1998, pp. 53–79.

[8] Scheeres, D. J., Ostro, S. J., Hudson, R. S., and Werner, R. A., "Orbits Close to Asteroid 4769 Castalia," *Icarus*, Vol. 121, No. 1, May 1996, pp. 67–87.

[9] Bettadpur, S. V., "Hotine's Geopotential Formulation: Revisited," *Journal of Geodesy*, Vol. 69, No. 3, 1995, pp. 135–142.
[10] Press, W. H., Flannery, B. P., Teukolsky, S. A., and Vetterling, W. T., "Numerical Recipes: The Art of Scientific Computing (FORTRAN Version)," Cambridge Univ. Press, New York, 1989, pp. 180–183, 554–560.
[11] Thomas, P. C., Binzel, R. P., Gaffey, M. J., Storrs, A. D., Wells, E. N., and Zellner, B. H., "Impact Excavation on Asteroid 4 Vesta: Hubble Space Telescope Results," *Science*, Vol. 277, No. 5331, 1997, pp. 1492–1495.

B. Marchand
Associate Editor